# Compound Cable-driven Parallel Robot for a Larger Wrench-feasible Workspace

Christine Chevallereau, Philippe Wenger, Stéphane Caro

# Compound Cable-driven Parallel Robot for a Larger Wrench-feasible Workspace

Christine Chevallereau, Philippe Wenger, and Stéphane Caro

Nantes Université, École Centrale Nantes, CNRS, LS2N, UMR 6004, F-44000 Nantes, France
{Christine.Chevallereau@ls2n.fr,Philippe.Wenger@ls2n.fr,Stephane.Caro@ls2n.fr}

**Abstract.** This article analyzes three versions of a planar *Compound Cable-Driven Parallel Robot* (CCDPR), which consists of a tensegrity mechanism mounted on the moving-platform (MP) of a overconstrained planar cable-driven parallel robot (CDPR). The main objective of the proposed solution is twofold: (i) to allow reaching areas near and even beyond its frame and (ii) to provide stiffness modulation for safe human interaction. The tensegrity mechanism embedded on the MP is an anti-parallelogram joint (X-mechanism) antagonistically actuated by cables. Three different X-mechanism actuation schemes are proposed: (i) actuation by two actuated winches embedded in the MP, (ii) remote actuation via two cable loops that also contribute to the motion of the MP and (iii) remote actuation via two independent cables. The resulting three CCDPRs are analyzed and compared to a single CDPR based on their wrench feasible workspace and an equilibrium robustness index, named capacity margin. The comparison is carried out for a practical case study where the task is to inspect walls and ceiling. We show that the CCDPRs perform better than the single CDPR.

**Keywords:** Cable-driven parallel robot, tensegrity, wrench-feasible workspace

## 1 Introduction

Cable-Driven Parallel Robots (CDPRs) are a subclass of parallel robots. CDPRs consist of a base frame and a moving-platform (MP) connected by cables. The movement of the platform is achieved by varying the cable lengths. CDPRs can have a large translational workspace [1], [2], a high payload capacity [3], be reconfigurable and portable [4], [5], [6], and perform high speed tasks [7]. However, the CDPR MP cannot generally go beyond the volume occupied by the cable exit points, except in special cases that take advantage of the platform's dynamic behaviour [8, 9].

In general, the workspace of parallel robots can be extended by combining them with other parallel or serial mechanisms to construct hybrid mechanisms. Some papers on CDPRs deal with this problem too. In [10], the authors propose a parallel spherical wrist actuated by cable-driven omni-wheels to overcome the inability of CDPR to achieve full-cycle rotations. In [11], the optimised design of a CDPR with an embedded tilt-roll wrist actuated by cables with remote actuators was presented.

In summary, the hybrid mechanism has both the advantages of the large workspace of the CDPR and overcomes the disadvantages of the CDPR well. It is appropriate to mount a serial robot on the MP to cover a large workspace with good dexterity. If the

mechanism installed on the platform is also controlled by cables, different concepts can be used for actuation. Among the cable-controlled joints, the mechanisms derived from the Snelson's X-shape mechanism have interesting properties in terms of low inertia [12], workspace size [13] and co-activity [14]. Therefore, it is relevant to investigate the performance of Compound Cable-driven Parallel Robots (CCDPRs) made up of a tensegrity mechanism embedded on a CDPR MP in terms of workspace size and equilibrium robustness.

This paper aims to analyse the wrench capability and workspace of CCDPRs. The proposed robot architectures are presented in Sec. 2. They differ depending on how the embedded mechanism, namely the X-mechanism, is actuated. First, the actuators of the X-mechanism are embedded on the MP, . Then, the X-mechanism is actuated by two independant cables connected on one end to the coupler link of the mechanism and to a remote actuator on the frame on the other end. Finally, the X-mechanism is actuated with two cables loops connected each to two remote actuators on the frame. In Sec. 3, the kinetostatic models of the manipulators under study are expressed and a robustness equilibrium index, named capacity margin, is recalled. The latter is used to trace the boundaries of the wrench-feasible workspace of the three CCDPRs under study. The three proposed CCDPRs are compared to a classical CDPR based on two specific tasks in Sec. 4. Finally, conclusions are drawn and future work is discussed in Sec. 5.

## 2 Description of the CCDPRs under study

The CCDPRs studied in this paper consist of a planar CDPR and an anti-parallelogram joint, called *X-mechanism*, mounted on the moving platform (MP) in the plane motion of the CDPR, as shown in Fig. 1.

The mass of MP is denoted as $m_P$ and its center of mass is located at point $P$. It is driven with four to six cables connecting exit points $A_i$ to anchor points $B_i$. The CCDPRs have four degrees of freedom (DOF): three are provided by the CDPR itself and an additional one is provided by the X-mechanism. Let $\mathbf{q} = [x, y, \phi, \alpha]^T$ define the configuration vector of the CCDPRs. $(x, y)$ are the Cartesian coordinates of point $P$, $\phi$ is the orientation angle of the MP with respect to the base frame and $\alpha$ is the orientation angle of the top bar of the X-mechanism with respect to the MP. The output coordinates are the two Cartesian coordinates $(x_E,\ y_E)$ of the end effector (EE) $E$, placed at the middle point of the top bar of the X-mechanism, along with its orientation angle $\alpha + \phi$ in the reference frame. The EE pose is denoted by $\mathbf{x} = [x_E, y_E, \phi + \alpha]^T$. For the sake of simplicity, the mass $m_T$ of the X-mechanism and of the payload is concentrated at point $E$. The X-mechanism is actuated by two cables attached to the ends of the top bar and pulling on each side via a small pulley of radius $r$. Springs are added to the ends of the top bar and the center of the pulley to achieve a stable configuration at rest. Accordingly, the CCDPRs are kinematically redundant. For a fully-actuated CDPR with $n$ degrees of freedom, $n + 1$ cables at least must be used to ensure that the cables are always taut. Thus five cables are required. Six cables are used in total, which means that the CCDPRs are also redundantly actuated. In this study, the extra cable is used to modulate the stiffness of the X-mechanism.

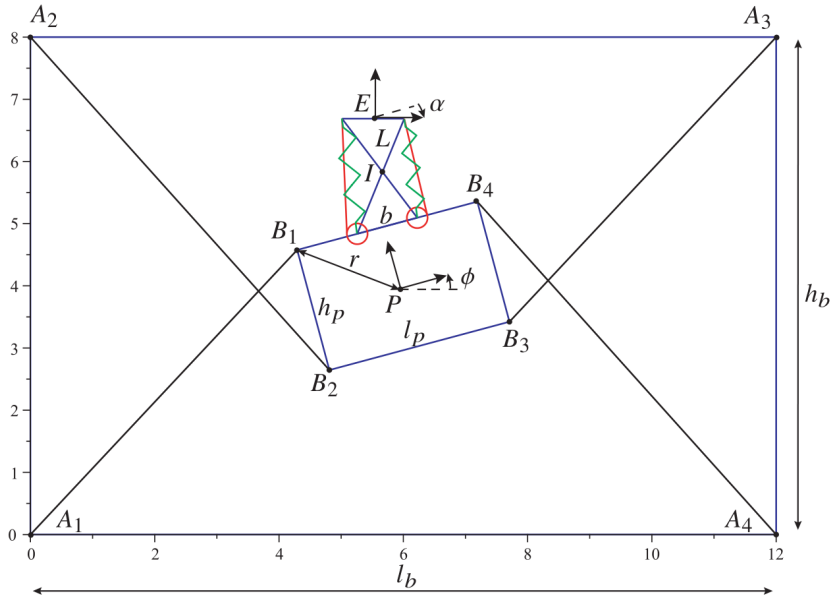


Fig. 1: CCDPR composed of a X-mechanism with actuators mounted on the CDPR MP

### 2.1 Concept 1: X-mechanism with actuators mounted on the CDPR MP

Figure 1 shows a CCDPR where the two antagonistic cables of the X-mechanism are actuated by two motorized winches embedded on the MP. Here, the CDPR MP is driven by four cables and the actuation of the X-mechanism is decoupled from the one of the CDPR MP. It should be noted that the total mass $m_p$ of the CDPR MP is increased due to the embedded actuators used to drive the X-mechanism.

### 2.2 Concept 2: X-mechanism actuated via two independent cables

In this actuation scheme, shown in Fig.2, the X-mechanism is remotely actuated via two cables $\mathscr{C}_5$ and $\mathscr{C}_6$. These cables connect two motorized winches located on the CDPR frame to the end points of the top bar of the X-mechanism, passing through pulleys attached to the MP. These pulleys, of radius $r_p$, are centered on two vertices $B_1$ and $B_4$ of the MP. The left (right, resp.) cable enters the pulley at point $B_5$ (resp. $B_6$). Here, cables $\mathscr{C}_5$ and $\mathscr{C}_6$ act simultaneously on the MP and the X-mechanism.

### 2.3 Concept 3: X-mechanism actuated with two cables loops connected each to two remote actuators

Here, two cable loops are used to remotely control both the MP and X-mechanism. The left (right, resp.) cable loop is actuated by two motorized winches $M_1$ and $M_5$ (resp. $M_2$ and $M_6$) fixed on the CDPR frame. The cable loop wraps around a pulley of radius $r_c$

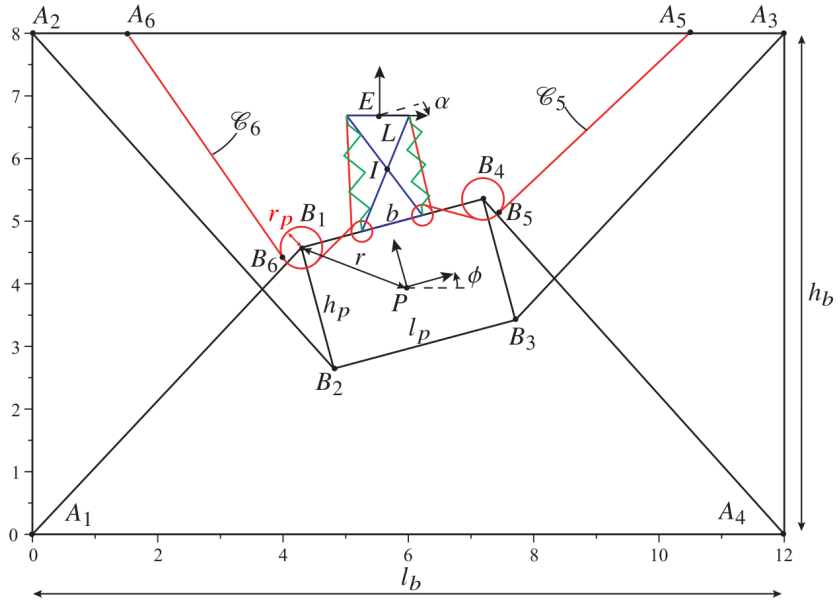


Fig. 2: CCDPR with a X-mechanism actuated by two independent cables

and the X-mechanism cable wraps around a pulley of radius $r_t$. As shown in Fig. 3, $r_c$ is the radius of the pulley connected to the cable loop (green pulley) and $r_t$ is the radius of the pulley connected to the X-mechanism cable (red pulley). The two above mentioned pulleys share the same axes and are mounted on the same shaft. The centers of the left and right pulleys are at the upper left corner $B_1$ and upper right corner $B_4$ of the MP, respectively. The MP twist is a function of the six remote actuator velocities, i.e., $M_1$ to $M_6$ velocities, whereas the X-mechanism top bar twist with respect to the MP frame is only a function of $M_1$, $M_4$, $M_5$ and $M_6$ velocities.

## 3 Wrench-feasible workspaces of the CCDPRs

The static equilibrium equation of the CCDPRs can be written in a matrix form as:

$$\boldsymbol{W}(\boldsymbol{q})\boldsymbol{t} + \boldsymbol{w_e}(\boldsymbol{q}) = \mathbf{0}_4 \tag{1}$$

This form is similar to the classical static model of a CDPR [15] or of a X-mechanism actuated by cables [14]. The wrench matrix $\boldsymbol{W}(\boldsymbol{q})$ is $4 \times 6$ since the CCDPR has 4 configuration variables and is actuated by 6 cables. $\boldsymbol{t}$ is the cable tension vector of dimension 6. Vector $\boldsymbol{w_e}(\boldsymbol{q})$ corresponds to the effect of gravity and springs on the equilibrium of the system. It can also include other possible external forces [15], but the current analysis is limited to tasks that do not include contact forces. The first two lines correspond to the force equilibrium of the MP and the X-mechanism. The third

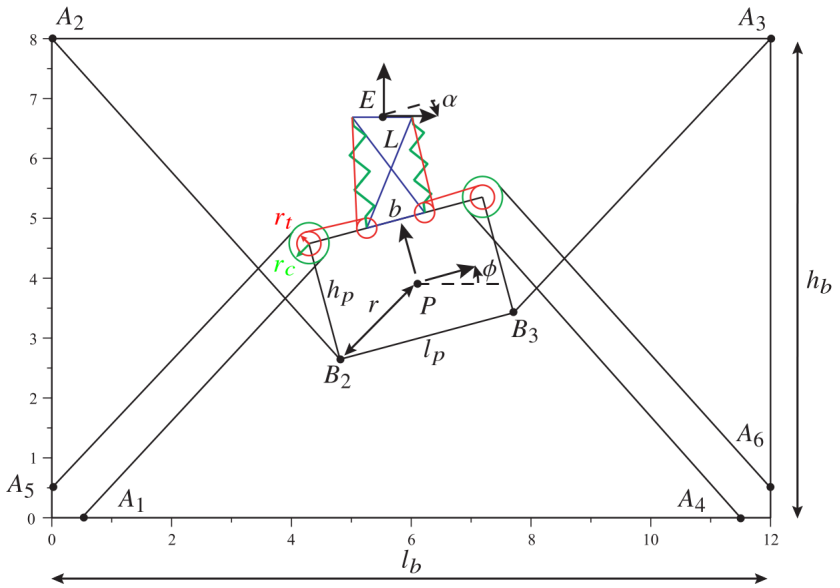


Fig. 3: CCDPR composed of X-mechanism actuated with two cables loops connected each to two remote actuators

line corresponds to the rotation equilibrium of the MP and the X-mechanism around P with respect to the frame. The fourth equation corresponds to the rotation equilibrium of the top bar of the X-mechanism around the instantaneous centre of rotation $I$ of the X-mechanism with respect to the MP. So that the terms of matrix $\mathbf{W}$ have the same unit, the third and fourth equilibrium equations are divided by the appropriate radius of gyration [16]. The cable tensions are all bounded between a minimum and positive tension $\underline{t}$ and a maximum tension $\bar{t}$. Formally, these limits define the six-dimensional box of feasible tensions:

$$\mathcal{T} = \{\boldsymbol{t} \in \mathbb{R}^6 / \underline{\boldsymbol{t}} \leq \boldsymbol{t} \leq \bar{\boldsymbol{t}}\} \tag{2}$$

The capacity margin is an index that measures how "safe" the robot is from going into an undesirable state, the index is denoted as $\gamma$. It is used to evaluate the robustness of equilibrium [15] for a given configuration $\mathbf{q}$. The capacity margin takes the minimum distance between the boundary of the polytope $\mathscr{W}_t$ and $-\boldsymbol{w_e}(\boldsymbol{q})$, where $\mathscr{W}_t$ is the Available Forces and Moments Set (AFMS). AFMS is the set of forces and moments (around P with respect to the frame and $I$ with respect to the MP frame) that the robot can produce for a given configuration, it can be defined as:

$$\mathscr{W}_t = \{\boldsymbol{w} \in \mathbb{R}^4 / \exists \boldsymbol{t} \in \mathcal{T}, \boldsymbol{w} = \boldsymbol{W}\boldsymbol{t}\} \tag{3}$$

The capacity margin $\gamma(\mathbf{q})$ can be calculated as the shortest signed distance from the $-\boldsymbol{w}_e$ to the nearest facet of $\mathscr{W}_t$. If the capacity margin is positive then $-\boldsymbol{w}_e$ is inside $\mathscr{W}_t$ and the pose $\mathbf{x}$ corresponding to the configuration $\mathbf{q}$ belongs to the Wrench Feasible

Workspace (WFW). If $-\boldsymbol{w}_e$ is outside $\mathscr{W}_t$, the capacity margin $\gamma(\mathbf{q})$ is negative and the configuration studied $\mathbf{q}$ cannot be maintained.

The WFW $\mathscr{F}$ is defined as:

$$\mathscr{W} = \{\mathbf{x} \in \mathbb{R}^2 \times SO(2) / \mathbf{x} = \mathbf{f}(\mathbf{q}) \text{ and } \gamma(\mathbf{q}) \geq 0\} \tag{4}$$

where $\mathbf{f}$ is the geometric function that relates the components of $\mathbf{q}$ and $\mathbf{x}$. The presence of the X-mechanism makes the CCDPR kinematically redundant. It means that a given pose of the EE can be reached with various orientation of the MP. For each pose $\mathbf{x}$, the configuration $\mathbf{q}$ corresponding to the largest capacity margin is considered. Let us define $\boldsymbol{Q}(\mathbf{x}) = \{\mathbf{q} / \mathbf{x} = \mathbf{f}(\mathbf{q})\}$. To build the WFW, we then define a capacity margin at a pose $\mathbf{x}$ as follows:

$$\gamma_X(\mathbf{x}) = \max_{\mathbf{q} \in \boldsymbol{Q}(\mathbf{x})} \gamma(\mathbf{q}) \tag{5}$$

Accordingly, the WFW can be also defined as:

$$\mathscr{W} = \{\boldsymbol{x} \in \mathbb{R}^2 \times SO(2) / \gamma_X(\mathbf{x}) \geq 0\} \tag{6}$$

Hence, the boundary of WFW amounts to $\gamma_x(\boldsymbol{x}) = 0$. Note that the WFW is crucial for design, control and planning tasks. It also provides insights into the poses for which the robot can safely operate.

In the following sections, the WFW of the three CCDPRs are computed. The results are compared to the WFW of a planar CDPR.

## 4 Wrench-Feasible Workspace Analysis of the three proposed CCDPRs

For better readibility, the WFWs are traced for a prescribed end-effector (EE) orientation. Two tasks are considered: (*i*) ceiling inspection with end-effector orientation $\alpha + \varphi = 0$ deg; (*ii*) wall inspection with end-effector orientation $\alpha + \varphi = 90$ deg. The obtained WFWs for the three CCDPRs are compared to the one of a planar CDPR, for which the EE is shifted by a length equal to the X-mechanism height at $\alpha = 0$. The EE is located at the top of the red line in Fig. 4(a). The parameter values of the CCDPRs under study are given in Table 1.

### 4.1 Ceiling inspection

For a prescribed orientation of the EE such that $\alpha + \varphi = 0$ deg, the WFWs of the three CCDPR and of the planar CDPR are shown in Fig. 4. The black dotted lines indicate the boundary of the CDPR frame and corresponds to the required working area. The upper dotted line corresponds to the ceiling. The contour lines represent the value of $\gamma_x$ defined in Eq. (5). The magenta line amounts to $\gamma_X = 0$ and corresponds to the workspace boundary.

For the CDPR, the orientation $\phi = 0$ deg of the MP is imposed, and for each pose of the EE, the capacity margin is shown in Fig. 4(a) where a significant part of the ceiling

Table 1: Parameter values used to compare the four manipulators

| | |
|---|---|
| Base frame length | $l_b = 6$ [m] |
| Base frame height | $h_b = 3$ [m] |
| MP length | $l_p = 0.5$ [m] |
| MP height | $h_p = 0.5$ [m] |
| Length of crossed bar of the X-mechanism | $L = 0.5$ [m] |
| Length of top bar of the X-mechanism | $b = 0.25$ [m] |
| MP mass | $m_P = 5$ [kg] for Concept 1 |
| | $m_P = 3$ [kg] for the other concepts |
| End-effector mass | $m_T = 2$ [kg] |
| Gravity constant | $g = 9.81$ $[m.s^{-2}]$ |
| Spring constants | $k_l = k_r = 190$ $[N.m^{-1}]$ |
| Free length of spring | $l_{sr0} = l_{sl0} = L - b$ |
| Radius of the pulley at the base of the X-mechanism | $r = 0.02$ [m] |
| Radius of the pulley attached to the platform | $r_P = r_c = 0.05$ [m] |
| Ratio of the two pulley radii for the cable loop | $\frac{r_c}{r_t} = 2$ |
| Cable tension lower bound | $\underline{t} = 0$ [N] |
| Cable tension upper bound | $\bar{t} = 120$ [N] |

can be reached, but not at the corners. An offset of the EE allows the framework of the CDPR to be partially bypassed.

For concept 1, a significant part of the ceiling can be reached as shown in Fig. 4(b), but some parts are not accessible. Note that for a MP mass equal to 3 kg, i.e. without considering the mass of the embedded actuators, the ceiling can be fully followed by the end-effector. For both concepts 2 and 3, the ceiling can be fully followed by the CCDPR end-effector as shown in Figs. 4(c) and 4(d).

### 4.2 Left wall inspection

The EE orientation is set as $\alpha + \varphi = 90$ deg. For the CDPR, the use of a simple offset of the EE, which was quite appropriate for the ceiling inspection task, is completely inappropriate for the left wall inspection task (see Fig. 5(a)). The weight of the tool creates a moment that significantly reduces the WFW size. Concepts 1 and 3 are able to perform the required task despite the extra weight due to the embedded motors for concept 1 (see Figs. 5(b) and (d)). This is not true for concept 2 as depicted in Fig. 5(c).

## 5 Conclusion

To increase the workspace size of a cable-driven parallel robot, in particular to allow it to go beyond the limits of its frame, it is possible to mount a serial robot on its moving-platform. In this paper, three novel robot architectures were introduced in order to enlarge the manipulator workspace such that the end-effector can go beyond the volume bounded by the cable exit points. Those robot architectures, named compound cable-driven parallel robots (CCDPRs) are made up of a classical cable-driven parallel

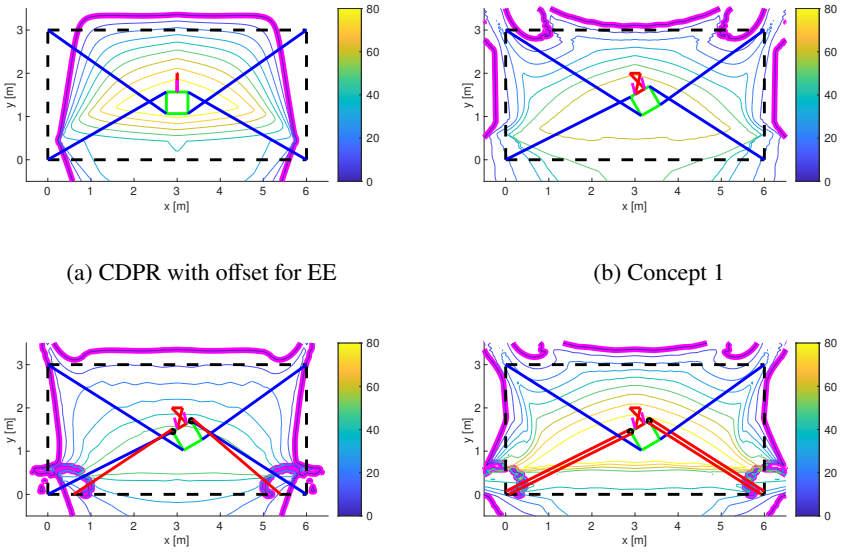


(a) CDPR with offset for EE

(b) Concept 1

(c) Concept 2

(d) Concept 3

Fig. 4: WFW of the four manipulators for $\varphi + \alpha = 0$ deg

robot (CDPR) with a tensegrity mechanism mounted on its moving-platform (MP). They differ depending on how the embedded mechanism, namely the X-mechanism, is actuated. First, the actuators of the X-mechanism are embedded on the MP. Then, the X-mechanism is actuated by two independant cables connected on one end to the coupler link of the mechanism and to a remote actuator on the other end. Finally, the X-mechanism is actuated with two cables loops connected each to two remote actuators. An analysis using heuristic placement of the attachment points and the dimensions of the mechanism revealed that the cable loop solution is the most relevant one among the studied manipulators. The obtained results should be validated based on design optimisation. The mechanism used is a system inspired by the concept of tensegrity, where antagonistic actuation and the presence of springs ensure equilibrium at rest and regulation of stiffness. Later on, the stiffness modulation allowed by the proposed CCDPRs will be studied and used to meet industrial needs.

**Acknowledgement**

This work was supported by ROBOTEX 2.0 (Grants ROBOTEX ANR-10-EQPX-44-01 and TIRREX ANR-21-ESRE-0015).

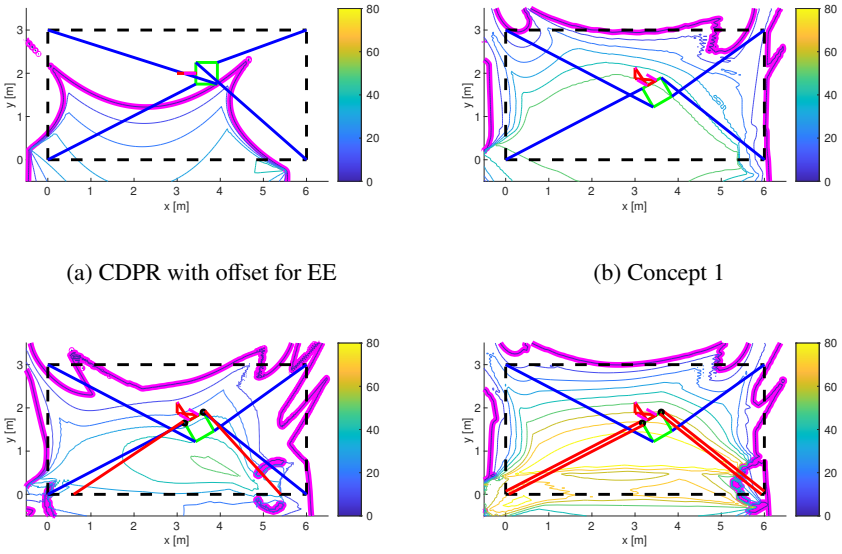


(a) CDPR with offset for EE

(b) Concept 1

(c) Concept 2

(d) Concept 3

Fig. 5: WFW of the four manipulators for $\varphi + \alpha = 90$ deg

## References


1. C. Lambert, M. Nahon, and D. Chalmers, "Implementation of an aerostat positioning system with cable control," *IEEE/ASME Transactions on Mechatronics*, vol. 12, no. 1, pp. 32–40, 2007.
2. P. Bosscher, R. L. Williams, L. S. Bryson, and D. Castro-Lacouture, "Cable-suspended robotic contour crafting system," *Automation in Construction*, vol. 17, no. 1, pp. 45–55, 2007.
3. R. Bostelman, J. Albus, A. Jacoff, J. Gross, and N. Pagalakis, *Applications of the NIST ROBOCRANE.* Robotics and Manufacturing, , -1, 1994-01-01 1994.
4. L. Gagliardini, S. Caro, M. Gouttefarde, and A. Girin, "Discrete reconfiguration planning for cable-driven parallel robots," *Mechanism and Machine Theory*, vol. 100, pp. 313–337, 2016.
5. T. Rasheed, P. Long, and S. Caro, "Wrench-Feasible Workspace of Mobile Cable-Driven Parallel Robots," *Journal of Mechanisms and Robotics*, vol. 12, p. 031009, 01 2020.
6. T. Rasheed, P. Long, A. S. Roos, and S. Caro, "Optimization based trajectory planning of mobile cable-driven parallel robots," in *2019 IEEE/RSJ International Conference on Intelligent Robots and Systems (IROS)*, pp. 6788–6793, 2019.
7. S. Kawamura, H. Kino, and C. Won, "High-speed manipulation by using parallel wire-driven robots," *Robotica*, vol. 18, no. 1, p. 13–21, 2000.
8. X. Jiang, E. Barnett, and C. Gosselin, "Dynamic point-to-point trajectory planning beyond the static workspace for six-dof cable-suspended parallel robots," *IEEE Transactions on Robotics*, vol. 34, no. 3, pp. 781–793, 2018.
9. G. Mottola, C. Gosselin, and M. Carricato, "Dynamically feasible motions of a class of purely-translational cable-suspended parallel robots," *Mechanism and Machine Theory*, vol. 132, pp. 193–206, 2019.

10. A. Platis, T. Rasheed, P. Cardou, and S. Caro, *Isotropic Design of the Spherical Wrist of a Cable-Driven Parallel Robot*, pp. 321–330. Cham: Springer International Publishing, 2018.
11. S. Lessanibahri, P. Cardou, and S. Caro, "A Cable-Driven Parallel Robot With An Embedded Tilt-Roll Wrist," *Journal of Mechanisms and Robotics*, vol. 12, p. 021107, 02 2020.
12. M. Arsenault and C. M. Gosselin, "Kinematic, static and dynamic analysis of a planar 2-dof tensegrity mechanism," *Mechanism and Machine Theory*, vol. 41, no. 9, pp. 1072–1089, 2006.
13. P. Wenger and D. Chablat, "Kinetostatic analysis and solution classification of a class of planar tensegrity mechanisms," *Robotica*, vol. 37, no. 7, pp. 1214–1224, 2019.
14. V. Muralidharan, N. Testard, C. Chevallereau, A. Abourachid, and P. Wenger, "Variable Stiffness and Antagonist Actuation for Cable-Driven Manipulators Inspired by the Bird Neck," *Journal of Mechanisms and Robotics*, vol. 15, p. 035002, 04 2023.
15. A. L. Cruz Ruiz, S. Caro, P. Cardou, and F. Guay, "Arachnis: Analysis of robots actuated by cables with handy and neat interface software," *Mechanisms and Machine Science*, vol. 32, 08 2015.
16. F. Guay, P. Cardou, A. L. Cruz-Ruiz, and S. Caro, "Measuring how well a structure supports varying external wrenches," Jan 2014.